Modeling Lidar Waveforms in Heterogeneous and Discrete Canopies

Wenge Ni-Meister, David L. B. Jupp, and Ralph Dubayah

Abstract—**This study explores the relationship between laser waveforms and canopy structure parameters and the effects of the spatial arrangement of canopy structure on this relationship through a geometric optical model. Studying laser waveforms for such plant canopies is needed for the advanced retrieval of three-dimensional (3-D) canopy structure parameters from the vegetation canopy lidar (VCL) mission.**

For discontinuous plant canopies, a hybrid geometric optical and radiative transfer (GORT) model describing the effects of 3-D canopy structure parameters of discrete canopies on the radiation environment has been modified for use with lidar. The GORT model is first used to describe the canopy lidar waveforms as a function of canopy structure parameters and then validated using scanning lidar imager of canopies by echo recovery (SLICER) data collected in conifer forests in central Canada during the boreal ecosystem–atmosphere study (BOREAS).

Model simulations show that the clumping in natural vegetation, such as leaves clustering into tree crowns causes larger gap probability and smaller waveforms for discontinuous plant canopies than for horizontally homogeneous plant canopies. Ignoring the clumping effect can result in significantly lower values for the estimated foliage amount in the profile and in turn lower estimated biomass. Because of clumping, only the gap probability and apparent vertical projected foliage profile can be directly retrieved from the canopy lidar data. The retrieval is sensitive to the ratio of the volume backscattering coefficients of the vegetation and background, and this ratio depends on canopy architecture as well as foliage spectral characteristics. Extensions of the GORT model from single-layered canopies to include multilayered ones are also explored.

Index Terms—**Geometric optical and radiative transfer (GORT) model, heterogeneous plant canopies, lidar waveforms.**

NOMENCLATURE

Roman Alphabet

b	Vertical crown radius (m).
F_a	Foliage area volume density of a single crown (m^{-1}).
$F_{app}(z)$	Apparent foliage profile as a function height z (m^{-1}).
$F_{act}(z)$	Actual foliage profile as a function height z (m^{-1}).
$G(z, \theta_i)$	Leaf area projection factor.
h, z	Certain height within the canopies (m).
h_c	Crown center height.
h_1	Lower bound of the crown centers (m).
h_2	Upper bound of the crown centers (m).
J_0	Emitting laser pulse energy (W).
$P(z)$	Total gap probability for a beam at nadir at height z.
$P(n = 0\|z, \theta_i)$	Between-crown gap probability for a beam at θ_i reaching height z.
$P(n > 0\|z, \theta_i)$	Within-crown gap probability for a beam at θ_i reaching height z.
$P_\lambda(h)$	Vertical crown density distribution function at height h (m^{-2}).
$p(\xi)$	Volume-scattering phase function of medium as a function of scattering angle.
R	Horizontal crown radius (m).
R_g	Lidar energy return from background within a footprint (W).
$R_v(z)$	Integrated lidar energy return within a footprint from canopy top to height z (W).
r	Leaf reflectance.
t	Leaf transmittance.

Greek Alphabet

λ	Crown count density (m^{-2}).
ρ_v	Volume backscattering coefficient of vegetation elements.
ρ_g	Volume backscattering coefficient of background.
$\tau(\theta)$	Projected foliage area volume density at direction θ (m^{-1}).
θ_i	Solar zenith angle.
θ_v	Viewing zenith angle.
ϕ_i	Solar azimuth angle.
ϕ_v	Viewing azimuth angle.
ξ	Scattering angle.
ω	Scattering albedo of leaves.
ω_g	Scattering angle.

Manuscript received July 31, 2000; revised December 27, 2000. This work was supported in part by NASA under Contract NAS597160 for the implementation of the VCL mission.

W. Ni-Meister is with Goddard Earth Sciences and Technology Center, NASA Goddard Space Flight Center, Greenbelt, MD 20771 USA (e-mail: wenge@land-gsfc.nasa).

D. L. B. Jupp is with CSIRO EOC, GPO Canberra 2601, Australia (e-mail: david.jupp@eoc.csiro.au).

R. Dubayah is with the Department of Geography, University of Maryland, College Park, MD 20742-8225 USA (e-mail: rdubayah@geog.umd.edu).

Publisher Item Identifier S 0196-2892(01)07611-2.

I. INTRODUCTION

IN ATMOSPHERE–VEGETATION interactions, the horizontal and vertical three-dimensional (3-D) canopy structure plays an important role. The radiation regime above,

within, and below plant canopies, which is the energy source for the exchange of heat, mass, and carbon in land surface, is fully driven by the horizontal and vertical dispersion of canopy elements. In addition, land surface roughness affects the exchanges of mass, energy and momentum between forest canopies and the lower atmosphere.

Measuring 3-D canopy structure from the ground is difficult and time consuming. Remote sensing, including passive and active remote sensing, provides a technically consistent means for estimating many landsurface biophysical parameters at large regional to global scales. However, most passive remote sensing systems, although mapping the horizontal organization of canopies, do not provide direct information on the vertical distribution of canopy elements. Furthermore, measurement of or accounting for ground topography in densely vegetated areas is either not possible or very difficult using traditional remote sensing methods.

Recent technologies based on laser lidar systems have the potential to overcome these problems. The systems being used in the design of the spaceborne vegetation canopy lidar (VCL), the current airborne laser vegetation imaging sensor (LVIS), and the previous scanning lidar imager of canopies by echo recovery (SLICER) have shown great promise and capacity to retrieve 3-D canopy structure information [3], [4]. Key objectives of VCL, LVIS, and SLICER are to provide estimates of not only canopy height and canopy structure parameters but possibly also of biomass and volume [3], [4], [12], [13], [16], [20]. Data from large-footprint scanning lidars will soon become much more widely available with the launch of the VCL [3]. Over its 18-month lifetime, this NASA instrument will acquire global data on forest structure.

These lidar systems use a laser system with large diameter footprints, (10–15 m for SLICER and 25 m for VCL and LVIS). A laser pulse at 1.064 μm is fired directly from zenith to nadir and reflected by the land surface and structures such as vegetation above it. The time elapsed since the pulse was fired measures the distances to scattering events and the terrain surface. A laser waveform is formed by recording the laser energy return as a function of time. The waveform is a function of canopy height and vertical distribution of foliage, as it is made up of the reflected energy from the surface area of canopy components such as foliage, trunks, twigs, and branches, at varying heights within the large footprint. The total waveform is therefore a measure of both the vertical distribution of vegetation surface area and the distribution of the underlying ground height.

Canopy structure parameters as well as ground elevation can be directly derived from the laser waveforms. For example, *ground elevation* is calculated from the elevation of the peak of the last return in the waveform, which is the reflection from the ground. *Canopy height* can be calculated as the distance between the first significant return above threshold and the ground [28], [21], [16], [12], [13], [4]. *Canopy cover*, the fraction of background obscured by vertically projected foliage and woody area above a certain height, is calculated by the cumulative laser returns from the canopy to that height divided by the total returns from the canopy and the ground adjusted by a ratio to account for differences in ground and canopy reflectance at 1.064 μm [12], [13]. Cumulative canopy height profile (CHP) is calculated by using a logarithmic transformation of (1-canopy cover), and relative CHP is computed by differencing CHP and dividing by total canopy CHP [12], [13], [8]. Close relationships have been found between such derived parameters from laser waveforms and field measurements. However, the relationships are generally empirical and the predicted parameters based on the relationships are often compared with field data based on measurements of the same type.

A physical model describing the laser photon interaction with plant canopies can be used to explore the relationship between lidar waveforms and 3-D canopy structure parameters. Some recent studies have modeled laser beam interaction with plant canopies using ray tracing techniques [6], [29], that require knowledge of the exact tree size, shape, and the exact location of each tree, which is difficult to obtain in practice.

A simpler canopy radiation model which can characterize the waveforms as a function of the statistical parameters of the tree geometry at the the scale of forest stands may be more useful in the application of lidar remote sensing for forest characterization. A tree "stand" is an area covered by trees from the same species association with similar basic spatial and functional arrangements. In forestry, for example, stands usually have a specific age class or distribution. VCL and LVIS with 25 m footprint and SLICER with a 10 m footprint are designed to measure canopy structure information at the integrated tree stand level. Such aggregated canopy radiation models are well suited for the study of the VCL, LVIS, and SLICER missions.

The objective of this study is to adapt a simple stand-based radiation model to characterize laser waveforms from plant canopies as a function of canopy structure parameters within large footprints. For homogeneous plant canopies, Beer's Law has often been used. However, for discontinuous natural vegetation, a geometric-optical and radiative transfer (GORT) approach is more suitable.

The GORT model was originally developed to model the bidirectional reflectance of discontinuous plant canopies [35]. It has been modified for modeling the solar radiation transmission and absorption by canopy elements [22]. Using the geometric optics (GO) approach, the clumping of leaves into tree crowns for discontinuous plant canopies is well described. The hierarchical clumping structure of plant canopies, including the clumping of needles into shoots, shoots into branches, branches into whorls, and whorls into crowns for conifer forests, has been found to be well modeled by GORT [22]. The radiative transfer (RT) component of the model characterizes the multiple scattering within the canopies. The GORT model has been applied and validated in conifer forests for photosynthetically active radiation (PAR) transmission, solar radiation transmission [22], bidirectional reflectances [23], [27], surface albedo [26], and spatial variances of remote sensing imageries [24], [25].

The GORT model is different from ray tracing models in that it models the integrated radiation regime within plant canopies at tree stand scale. The inputs are distribution functions of tree geometry parameters (such as mean tree size, shape and density) and the spectral properties of canopy elements and background. This integrated approach corresponds to the way in which foresters and ecologists take measurements in fixed and

variable plots, and it suited well to study the large-footprint lidar systems.

In this study, we use the GORT model to describe the lidar waveforms as functions of tree geometry parameters, and to study the effects of the clumping in natural vegetation on the relationship of laser waveforms and canopy structure parameters. We begin by developing the basic canopy lidar equations.

II. Background

A. Basic Canopy Lidar Equation

Let $P(z)$ denote the probability that there is a gap above height z in a canopy. For laser beams over a large footprint entering the canopy from the top, the expected proportions of the attenuated laser beams over the footprint at height levels z and $z-\Delta z$ are $P(z)$ and $P(z-\Delta z)$. $P(z)-P(z-\Delta z)$ is the expected proportion of laser energy intercepted by the canopy elements within the thin layer of width Δz. When Δz approaches zero, $\lim_{\Delta z\to 0}(P(z)-P(z-\Delta z)/\Delta z) = (dP(z)/dz)$ is the beam interception density. The intercepted laser beams are reflected by the canopy elements and returned back to the receiver.

Assume $R_v(z)$ is the integrated laser energy return from canopy top to height z, $R_v(0)$ is the integrated laser energy return from top to the bottom of the vegetation layer, R_g is the laser energy return from the ground, J_0 is the beam irradiance, ρ_g is the backscattering coefficient of the ground, and ρ_v is the volume backscattering coefficient of the basic canopy foliage element. Then the basic canopy lidar equations are

$$-\frac{dR_v(z)}{dz} = J_0\rho_v\frac{dP(z)}{dz} \tag{1}$$

$$R_g = J_0\rho_g P(0) \tag{2}$$

where $dR_v(z)/dz$ is the lidar energy return density within the canopy layer.

The term J_0 must be modeled explicitly since systems such as SLICER, VCL and LVIS are operated in a way that allows the emitted laser pulse energy to be modified over different surfaces (i.e., water versus forest) [Blair, personal communication].

Equation (1) can also be rewritten as

$$-\frac{dR_v(z)}{dz} = J_0\rho_v\frac{dP(z)}{dz} = J_0\rho_v F_{app}(z)P(z) \tag{3}$$

where $F_{app}(z)$ is called here the "apparent foliage profile," which we have defined as

$$F_{app}(z) = \frac{1}{P(z)}\frac{dP(z)}{dz} = \frac{d\log P(z)}{dz}. \tag{4}$$

Note that F_{app} is related to the relative canopy height profile (relative CHP) as used by [12], [13], [8]. The relative CHP will be denoted here by F^*_{app} and is defined in terms of $F_{app}(z)$ as

$$F^*_{app}(z) = \frac{F_{app}(z)}{\int_{z_1}^{z_2} F_{app}(z')dz'} \tag{5}$$

where z_1 and z_2 are the heights of the lower and upper boundary of the canopy layer. The interpretation of $F_{app}(z)$ and $F^*_{app}(z)$ in terms of the vertical distribution of canopy elements is discussed later.

Note that (1) is different from the atmospheric lidar model [19], which was applied by Sun and Ranson [34] for canopy lidar. The atmospheric lidar model is a two-way attenuation model, since the atmospheric elements (molecules or aerosols) are small and do not occlude radiation. However, for plant canopies, canopy elements such as leaves, twigs, and branches are large enough to cast shadows. Because all shadows in the direction of the incident pulse are occluded, the laser beams are scattered preferably back to the same direction as the incident beams, i.e., to the backward direction. For the current lidar system, the laser beam therefore has a peak return from nadir. This is the so-called hotspot effect [7]. In this case, a one-way attenuation model is used because a scattering surface that can be reached by laser energy will also be "visible" to the receiver. In the future, if a lidar system is used that can receive the returned laser energy in a direction different from the incident beam direction, a hot spot interaction term as a function of incident and returned directions must be added to (1). The use of such bistatic lasers (although not lidars) to plant canopy analysis has been described by [11].

The volume backscattering coefficient of a canopy element ρ_v is a function of leaf angular distribution, phase function of leaf scattering, and spectral properties (e.g., leaf transmittance and leaf reflectance). If the phase function of the foliage elements depend only on scattering angle, it can be written as

$$\rho_v = \frac{p(\xi)}{4\pi}\omega\pi \tag{6}$$

where $(p(\xi)/4\pi)\omega$ is the bidirectional reflectance distribution function (BRDF) at the unit of sr^{-1}. To convert it to reflectance units (unitless), a constant π sr is applied. ω is the single scattering albedo of leaves, with $\omega = r + t$, where r and t are the leaf reflectance and transmittance. $p(\xi)$ is the volume scattering phase function of plant canopies with

$$\int_{4\pi}\frac{p(\xi)}{4\pi}\,d\Omega = 1. \tag{7}$$

$d\Omega$ is the solid angle element, ξ is the scattering angle

$$\cos\xi = \cos\theta_i\cos\theta_v + \sin\theta_i\sin\theta_v\cos(\phi_i - \phi_v) \tag{8}$$

where (θ_i, ϕ_i) are the zenith and azimuth angles of the incident beam direction, and (θ_v, ϕ_v) are the zenith and azimuth angles of the scattered direction. For plant canopies, $p(\xi)$ is a function of spectral scattering coefficients of leaves and their orientation distribution [30].

For randomly oriented lambertian leaves

$$p(\xi) = \frac{8}{\omega}\left(\frac{\omega}{3\pi}(\sin\xi - \xi\cos\xi) + \frac{t}{3}\cos\xi\right). \tag{9}$$

For vertical lambertian leaves

$$p(\theta_i, \theta_v, \Delta\phi) = \frac{8\sin\theta_i\sin\theta_v}{\omega} \cdot\left(\left(\frac{\omega}{2\pi}(\sin\Delta\phi - \Delta\phi\cos\Delta\phi) + \frac{t}{2}\cos\Delta\phi\right)\right. \tag{10}$$

where $\Delta\phi = \phi_v - \phi_i$ with $0 \le \Delta\phi \le \pi$.

For horizontal lambertian leaves

$$p(\theta_i, \theta_v) = \begin{cases} r|\cos\theta_i \cos\theta_v|, & \text{leaf surface intersects } \xi \\ t|\cos\theta_i \cos\theta_v|, & \text{otherwise.} \end{cases} \tag{11}$$

Since the laser return is at the hotspot ($\xi = 0$) for randomly oriented lambertian leaves, we have

$$p(\xi) = \frac{8t}{3\omega}. \tag{12}$$

For green vegetation $r = 0.6\omega$, $t = 0.4\omega$ for $\omega < 0.5$, otherwise $r = 0.7\omega$, $t = 0.3\omega$ [31]. At 1.064 μm, $\omega > 0.5$ [30] for green plant canopy. Thus, we have $p(\xi) = 0.8$. Equation (6) becomes

$$\rho_v = \frac{\omega}{5}. \tag{13}$$

To parameterize the volume backscattering coefficient of the ground ρ_g and we assume the ground is a Lambertian surface, then $p(\xi)$ is written as

$$p(\xi) = \begin{cases} 2 & \xi \le \frac{\pi}{2} \\ 0 & \text{otherwise.} \end{cases} \tag{14}$$

Assume ω_g is the single scattering albedo of the ground, then

$$\rho_g = \frac{p(\xi)}{4\pi}\omega_g \pi. \tag{15}$$

For backscattering

$$\rho_g = \tfrac{1}{2}\omega_g. \tag{16}$$

From (13) and (15), we obtain

$$\frac{\rho_v}{\rho_g} = \frac{2}{5}\frac{\omega}{\omega_g}. \tag{17}$$

For vertical lambertian leaves

$$\frac{\rho_v}{\rho_g} = 0. \tag{18}$$

For horizontal lambertian leaves

$$\frac{\rho_v}{\rho_g} = \begin{cases} \dfrac{r}{2}\dfrac{\omega}{\omega_g}, & \text{leaf surface intersects } \xi \\ \dfrac{t}{2}\dfrac{\omega}{\omega_g}, & \text{otherwise.} \end{cases} \tag{19}$$

As we have seen in the previous equations, the lidar energy return is a function of laser pulse energy, the vertical distribution of gap probability, the spectral properties (such as single scattering albedo of leaves) of the canopy elements, their angular orientations, and the spectral properties of the ground.

B. Retrieving Gap Probability and Apparent Foliage Profile

As shown in the basic lidar equations, the laser energy returns can be directly related to the gap probability $P(z)$. In practice, the broadened laser beam is attenuated and reflected by foliage elements at different heights and provides us with the means to estimate $P(z)$ from the recorded waveform. With a knowledge of the backscattering coefficient of the plant canopy, ρ_v, and atmospherically corrected laser pulse energy J_0, the estimated gap probability can be directly retrieved from the lidar waveform as

$$P(z) = 1 - \frac{R_v(z)}{J_0\rho_v}. \tag{20}$$

As previously defined, $R_v(z)$ is the accumulated laser energy return from the canopy top to height level z within the canopy layer. This can be directly obtained from the lidar waveform. However, J_0 is not always available since the data are often not calibrated and the outgoing pulse power is often not measured reliably. It therefore may be hard to retrieve the vertical profile only from (20).

Nevertheless, by using the ground return as a reference and with some knowledge of the ground and foliage reflectance ratio it is possible to obtain $P(z)$ from uncalibrated data using the following three equations

$$R_g = J_0\rho_g P(0) \tag{21}$$

$$R_v(0) = J_0\rho_v(1 - P(0)) \tag{22}$$

$$R_v(z) = J_0\rho_v(1 - P(z)). \tag{23}$$

Combining these we have

$$P(z) = 1 - \frac{R_v(z)}{R_v(0)}\frac{1}{1 + \dfrac{\rho_v}{\rho_g}\dfrac{R_g}{R_v(0)}}. \tag{24}$$

$R_v(z)$, $R_v(0)$ and R_g are the laser energy returns from the canopy top to height z, from canopy top to ground, and from the ground return individually. Their ratios $R_v(z)/R_v(0)$ and $R_g/R_v(0)$ can easily be calculated from the lidar waveform. Thus, with the knowledge of ρ_v/ρ_g, $P(z)$ can be retrieved from an uncalibrated canopy lidar waveform.

From $P(z)$, apparent and relative foliage profiles can be estimated from (4) and (5). Replacing $P(z)$ in (4) and (5) by (24), we notice that $F_{app}(z)$ is quite sensitive to the value of ρ_v/ρ_g, but $F^*_{app}(z)$ is not. The reason is that the effect of ρ_v/ρ_g appears in both numerator and denominator in $F^*_{app}(z)$, in agreement with [12] and [13].

It follows that, in addition to the canopy height, which is a straightforward product from laser waveforms, a vegetation lidar system can provide gap probability $P(z)$, the vertical profiles of canopy cover $1 - P(z)$, apparent foliage $F_{app}(z)$, and relative apparent foliage $F^*_{app}(z)$, provided ρ_v/ρ_g is known. These are the techniques commonly used to retrieve canopy structure parameters from lidar waveforms [14], [12], [13]. Note that ρ_v/ρ_g changes with leaf orientation factor and spectral properties of the leaves and background and will therefore often vary between stands.

Successful retrievals of canopy structure from canopy lidar data have been achieved using the above methods by assuming that $F_{app}(z)$ can be identified as the vertical profile of vertical projections of foliage elements, or the profile of vertical foliage area density. However, as observed by a number of authors, (4) can only give us an "apparent" foliage profile which will differ from the actual vertical foliage area density. The question is therefore: how well does the apparent foliage profile match with the actual foliage profile? Some factors in this difference are

the foliage orientation and canopy clumping. Different levels of clumping exist in different types of forests. In these cases, how different is the apparent foliage profile from the actual foliage profile? In what situations does the apparent foliage profile match the actual foliage profile? Will a biased foliage profile lead to biased biomass retrieval? To answer the above questions, models describing gap probability by 3-D canopy structure parameters for different spatially arranged plant canopies, are presented next.

III. Canopy Structure and Gap Probability Models

The directional gap probability function for a canopy is defined as the probability of incoming beams at incident zenith angle θ_i and azimuth angle ϕ_i reaching a given point located at a certain height in the canopy without being scattered. It is denoted $P(z, \theta_i, \phi_i)$. The gap probability is the key concept for modeling lidar waveforms as it links canopy structure with the lidar waveforms through the lidar equation.

A. Canopy Structure

The attenuation of laser beam irradiance passing through a canopy is directly affected by the density, size, and distribution (horizontal and vertical) of foliage and woody elements within the canopy, as well as spectral and roughness properties of leaves, wood elements, and the surface beneath the canopy. In general, the basic foliage and woody elements are assumed to be relatively small with area volume density (sum of areas of elements with "centers" in unit volume) and orientation volume density (distribution function of elements with centers in unit volume) that may vary vertically or horizontally.

From the study of point patterns, which reside with the dispersion of the centers of the objects, [10] and [30] suggested three dispersions to describe the distribution of the centers of the foliage and woody elements: regular (e.g., plantation) or semi-regular (e.g., row crops), random, and clumped (or clustered).

The "random" or Poisson point process is generally the null hypothesis where there is an equal probability of finding a plant at any location with an equal probability. If the point pattern is more clustered than the Poisson case, then variance is higher than the mean, the distribution of the individuals in subsets is broader and the distances from individuals to near neighbors are lower than from arbitrary points. The opposite cases indicate that individuals are dispersed more regularly than "random." The distribution generated by the point process is called stationary if it is independent of arbitrary translations of the origin and isotropic if it is invariant under the arbitrary rotation about the origin. Stationary is often called "homogeneity."

Processes can be stationary (homogeneous) in given directions in planes and not in other directions and isotropic in planes without being isotropic in the whole space. Note, however, that a process can be stationary and isotropic, but still have spatial dependence and correlation that may lead to clustering and clumping of the points in the space.

Jupp [10] notes that the dispersion is scale-dependent and can be hierarchical with objects being composed of smaller objects and themselves having size, shape, orientation and dispersion. By using a hierarchical model the focus of issues such as "clumping" resolves to the dispersion of individuals within and between the elements of the hierarchy.

It is generally assumed that the centers of the phyto-elements are distributed with a Poisson point process that is homogeneous in the horizontal direction. Vertical homogeneity is not necessary or desirable since leaf density varies significantly with height in crops, grasslands, and forests. The independence properties of the Poisson are retained between layers that are thick enough for phyto-elements to be essentially only in one layer. This creates the need to assume small phyto-elements if differential equation models are to be used.

Random and clumped dispersions (e.g., natural stands) are often isotropic. In this case, the gap probability is only a function of the incident zenith angle in addition to height, and is written as $P(z, \theta_i)$. We only focus on the canopies with isotropic random and clumped dispersions since these represent areas that lidar has been applied to. The clumped dispersion is also called a "discontinuous" plant canopy.

The simplest case for random and clumped canopies is that of a single-species and single-layered canopy. However, multispecies and multilayered plant canopies are also common in reality. Here we only examine single-species and single-layered canopies. A more general gap probability model for multispecies and multilayered plant canopies will be presented in a separate study, but we will explain how the single-species and single-layered models can be extended to multispecies and multilayered cases.

B. Horizontally Homogeneous Canopies

For a horizontally random plant canopy, assume $P(z, \theta_i)$ is the gap probability, $F_a(z)$ is the foliage area volume density with a unit of m^2/m^3, defined as foliage area per unit volume. $F_a(z)$ is a function of height z, and is the actual foliage profile for a single-species horizontally random plant canopy. For a multispecies and multilayered plant canopy, the actual foliage profile is the summation of $F_a(z)$ for different species. $G(z, \theta_i)$ is the leaf area projection factor, which is defined as the projection of a unit foliage area at the incident zenith angle θ_i onto a plane perpendicular to the direction of beam travel [30]. $G(z, \theta_i)$ is a property of the foliage elements in addition to area

$$G(z, \theta_i) = \begin{cases} \frac{1}{2} & \text{uniformly random leaf orientation} \\ \cos\theta_i & \text{horizontal leaf orientation} \\ \frac{2}{\pi}\sin\theta_i & \text{vertical leaf orientation.} \end{cases} \tag{25}$$

The gap probability for a single-species and single-layered horizontally homogeneous plant canopy is derived as follows (see Fig. 1)

$$P(z+\Delta z, \theta_i) - P(z, \theta_i) = P(z+\Delta z, \theta_i)G(z, \theta_i)F_a(z)\frac{\Delta z}{\cos\theta_i}. \tag{26}$$

When Δz approaches zero, and using the definition of F_{app}

$$F_{app}(z, \theta_i) = \frac{d\log P(z,\theta_i)}{dz} = \frac{G(z,\theta_i)F_a(z)}{\cos\theta_i} \tag{27}$$

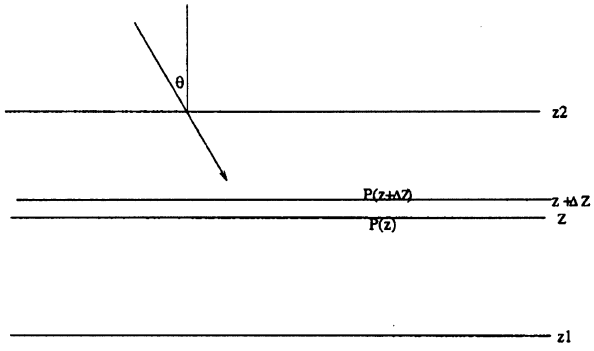

Fig. 1. Diagram for light attenuation in a horizontally homogeneous plant canopy.

and

$$P(z, \theta_i) = \exp\left(-\int_z^{z_2} G(z, \theta_i)F_a(z)\frac{dz}{\cos\theta_i}\right). \quad (28)$$

At the nadir case

$$F_{app}(z) = G(z, 0)F_a(z) \quad (29)$$

$$P(z) = \exp\left(-\int_z^{z_2} G(z, 0)F_a(z)dz\right). \quad (30)$$

The apparent foliage profile $F_{app}(z)$ is thus different from the actual foliage profile $F_{act}(z) = F_a(z)$, in this case, by the leaf area projection factor $G(z, 0)$.

C. Discontinuous Plant Canopies

As a means of modeling the clustering of foliage into tree crowns while still retaining the useful results obtained from random dispersion, it is possible to consider that the foliage elements are dispersed in the volumes defined by the crowns and the crowns are dispersed as discrete objects.

To derive the actual foliage profile for such plant canopies, assume first that we have uniform trees randomly distributed horizontally and with varying crown density vertically. $P_\lambda(h)$ is the vertical crown density distribution function in a unit of m^{-2}, and h is the height at crown center. $S(h, z)$ is the mean crown cross-section area at height z for trees with crown center height at h. With the foliage area volume density F_a, the actual foliage profile can be written as

$$F_{act}(z) = \int_{h_1}^{h_2} P_\lambda(h)F_a S(h, z)\, dh. \quad (31)$$

For canopies with more than one species, where each species has its own parameters, and assuming the different species and layers are independent, the actual foliage profile can be expressed as a summation of the species information

$$F_{act}(z) = \sum_i F_{act}(i, z) \quad (32)$$

where $F_{act}(i, z)$ is the actual foliage profile at height z for species i.

For the following two simple single-species and single-layered cases, the actual foliage profile can be determined exactly.

- Identical trees of ellipsoid shape with horizontal and vertical crown radii R and b are randomly distributed in space with crown count density λ, the center of the crowns is at a single height h

$$F_{act}(z) = \begin{cases} \lambda F_a \pi R^2 \left(1 - \left(\dfrac{z-h}{b}\right)^2\right), & \dfrac{|z-h|}{b} \le 1 \\ 0, & \text{otherwise.} \end{cases} \quad (33)$$

  The vertically projected actual foliage profile is the product of $G(z, 0)$ and $F_{act}(z)$.
- Identical trees with ellipsoid shape, with horizontal and vertical crown radii R and b, are randomly distributed in space with crown count density λ. The center of the crowns is uniformly located between height h_1 and h_2. $F_{act}(z)$ is: if $h_2 - b \le h_1 + b$

$$\begin{cases} \lambda F_a \pi R^2 \dfrac{(z+b-h_1)^2(h_1+2b-z)}{3b^2(h_2-h_1)}, \\ \quad h_1 - b \le z \le h_2 - b \\ \lambda F_a \pi R^2 \dfrac{3b^2 - (h_2-h_1)^2 - 3(z-h_2)(z-h_1)}{3b^2}, \\ \quad h_2 - b \le z \le h_1 + b \\ \lambda F_a \pi R^2 \dfrac{(h_2-z+b)^2(2b+z-h_2)}{3b^2(h_2-h_1)}, \\ \quad h_1 + b \le z \le h_2 + b \\ 0, \quad \text{otherwise.} \end{cases} \quad (34)$$

  Otherwise

$$\begin{cases} \lambda F_a \pi R^2 \dfrac{(z+b-h_1)^2(h_1+2b-z)}{3b^2(h_2-h_1)}, \\ \quad h_1 - b \le z \le h_1 + b \\ \lambda F_a \pi R^2 \dfrac{4}{3}\dfrac{b}{h_2-h_1}, \\ \quad h_1 + b \le z \le h_2 - b \\ \lambda F_a \pi R^2 \dfrac{(h_2-z+b)^2(2b+z-h_2)}{3b^2(h_2-h_1)}, \\ \quad h_2 - b \le z \le h_2 + b \\ 0, \quad \text{otherwise.} \end{cases} \quad (35)$$

1) Gap Probability for Single-Species and Single-Layered Discontinuous Canopies: For natural vegetation the different levels of clumping lead to a nonrandom dispersion of canopy elements. The clumping of leaves into crowns creates a nonuniform distribution of canopy gaps. Some proportion of the laser beam will pass through the canopy without passing through tree crowns [i.e., between-crown gaps, $P(n = 0)$ as shown in Fig. 2], while another proportion may pass through crowns without being scattered [within-crown gaps, $P(n > 0)$ as shown in Fig. 2]. The total canopy gap probability includes between-crown and within-crown gap probability.

In the GORT model, the discontinuous canopy layer is modeled as an assemblage of randomly distributed tree crowns of ellipsoidal shape, with a mean value of horizontal crown radius R and a mean value of vertical crown radius b and centers distributed uniformly between heights h_1 and h_2, where h_1 and h_2 are the

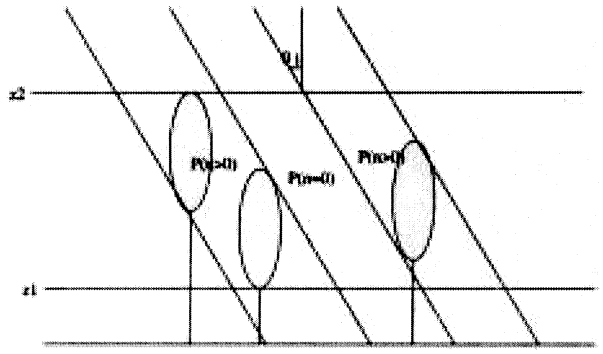

Fig. 2. Between-crown $P(n = 0)$ and within-crown $P(n > 0)$ gap probabilities.

lower and upper bounds of crown center height. λ is the stem count density in m^{-2}. The crown shape parameter b/R is assumed constant for any species. For example, our field measurements show that b/R is 3.5 for old jack pine forests and 2.9 for old black spruce forests in central Canada [22]. For shrublands in the Jornada site in Central New Mexico, b/R is very close to 1 [27]. Within each single crown, the foliage and branches can be uniformly distributed or nonrandomly distributed, for example, the horizontal whorl branch structure [22].

The between-crown gap probability $P(n = 0|z, \theta_i)$ is defined as the proportion of beams at incident zenith angle θ_i that reaches a point located at height z without passing through any crowns (i.e., $n = 0$). The between-crown gap probability was modeled using the Boolean Model [32] of mathematical morphology, which consists of random sets with centers that are Poisson distributed.

The within-crown gap probability $P(n > 0|z, \theta_i)$ is defined as the proportion of the laser beam passing through at least one crown without being scattered. The calculation of the within-crown gap probability is complex. The within-crown gap probability is modeled by the summation of the probabilities of the laser beam passing through 1, 2, 3..., n crowns. To model the gap probability of a laser beam passing through n crowns, the GORT model calculates the location where the laser beams enter crowns and the within-crown pathlength for each crown. A detailed description of the gap probability calculation can be found in [35] and [22].

For illustrative purposes, the gap probabilities for two scene A and B (see Fig. 3), were calculated using the GORT model. The tree geometry parameters for the GORT model are shown in Table I. Fig. 4 shows the modeled vertical distributions of gap probabilities, waveforms, and retrieved apparent foliage profiles.

The top two plots in Fig. 4 show the modeled total gap probability as a function of height using the GORT model. The total gap probability $P(z)$ includes the between-crown gap probability $P(n = 0, z)$ and the within-crown gap probability $P(n > 0, z)$, which are also shown in Fig. 4. The total gap probability from the GORT model has a sigmoid shape.

The between-crown gap probability $P(n = 0, z)$ shows a quick exponential decay in the upper part of the canopy. In the lower part of the canopy, the between-crown gap probability $P(n = 0, z)$ is almost constant. This can be understood by examining Fig. 3. Above the height $(h_1 + h_2)/2$, the between-crown gap probability $P(n = 0, z)$ decreases because of the increase of crown width. At height $(h_1+h_2)/2$, the crown width reaches a maximum and $P(n = 0, z)$ approaches a minimum value at height $(h_1 + h_2)/2$, constant at $z < (h_1 + h_2)/2$.

As the beam penetrates into crowns, $P(n > 0, z)$ increases, reaches a peak value, and then decreases. The proportion of incoming beam entering the crowns in a very thin layer at height z is $(dP(n = 0, z)/dz)$. The integrated laser beam entering the crown from canopy top to height z is $1 - P(n = 0, z)$. Part of the beam passing through the crown without hitting any crown elements forms the within-crown gap probability $P(n > 0, z)$. $P(n > 0, z)$ is almost zero at the top of the the canopy, since the integrated $(dP(n = 0, z)/dz)$ is small. As the laser beam penetrates into canopies, integrated $(dP(n = 0, z)/dz)$ increases, $P(n > 0, z)$ also increases. Meanwhile as the beams penetrate, an exponential decay of the beam inside crowns—a horizontally-homogeneous medium—also lessens the increase of $P(n > 0, z)$. Until at a certain level above $(h_1 + h_2)/2$, the factor of the exponential decay becomes the controlling factor, and $P(n > 0, z)$ decreases. The summation of between-crown gap probability, $P(n = 0, z)$ and within-crown gap probability, $P(n > 0, z)$ forms the sigmoid shape of total canopy gap probability.

The middle two plots in Fig. 4 show the vertical profile of $dP(z)/dz$, which is linearly related to the laser waveform by the volume scattering coefficient. A peak value is shown in the upper part of the canopy layer. The bottom two plots in Fig. 4 show the apparent foliage profile retrieved by taking the logarithmic transformation of gap probability. Because of the clumping effect, the actual total gap probability for discontinuous plant canopies is larger than the one for horizontally homogeneous plant canopies. This leads to an apparent foliage that is less than the actual foliage profile.

In summary, two factors contribute to the deviation of apparent foliage profile from the actual one. One factor is the leaf orientation, and the other is the clumping effect for natural vegetation. For a horizontally homogeneous canopy, only leaf orientation causes the difference. For natural vegetation, both factors are involved. We have shown that as a means to interpret the data, the gap probability can be directly retrieved from the lidar return with the knowledge of ρ_v/ρ_g. However, the relationship between the gap probability and the actual foliage profile for natural vegetation is complex. Unless we can separate the between-crown and within-crown gap probability, the actual foliage profile can not be directly retrieved from lidar data.

2) Gap Probability for Multispecies and Multilayered Discontinuous Canopies: For many forest stands, for example those in the tropics, a multilayered and multispecies model is required. The gap probability for multispecies and multilayered discrete canopies can be very complex. Here we show how we can extend the single-species and single-layered model to multispecies and multilayered model. Two canopies with single-layer and single species, have been chosen, one is the conifer forest, the other is a broadleaf forest. Fig. 4 shows the modeled gap probability $P(z)$, dP/dz for the conifer forest using the GORT model. Fig. 5 (left column) shows the modeled gap probability $P(z)$ and dP/dz for a single layer broadleaf

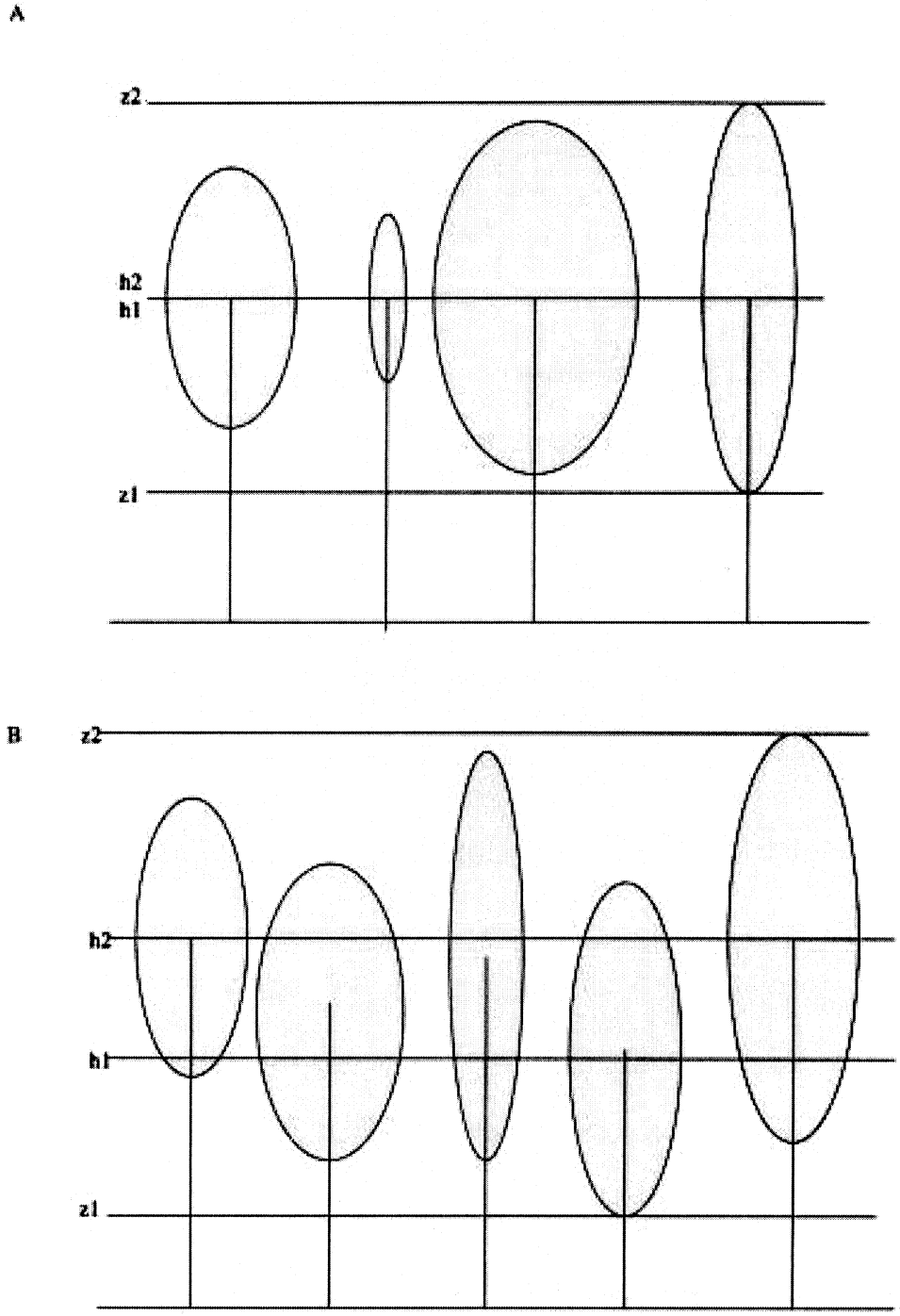

Fig. 3. Two cases of canopy structure. (a) Trees of different size randomly distributed in space with the crown centers located at height $h_1(h_2)$. (b) Trees of different size randomly distributed in space with the crown centers located between height h_1 and h_2. The lower and upper boundary are at height z_1 and z_2.

TABLE I
INPUT TREE GEOMETRY PARAMETERS FOR THE GORT MODEL FOR CASES A AND B SIMULATIONS

scene	$R(m)$	$b(m)$	$\lambda(\frac{1}{m^2})$	$h_1(m)$	$h_2(m)$	$F_a(1/m)$
A	1.2	3.6	0.24	8	8	0.44
B	1.2	3.6	0.24	6	12	0.44

forest using the GORT model. The tree geometry parameters from tropical forests, in La Selva, are used [15] (see Table II).

The two-layered forest stand is constructed as follows. The conifer forest trees as used in Fig. 4 are located at the lower layer, and the broadleaf forest trees, as shown earlier, are located in the upper part of the canopy. If the tree distributions of these two species are independent of each other, the modeled gap probability, waveform, and the retrieved apparent foliage profile using the GORT model are shown in the right-hand column of Fig. 5. Two peaks appear in the laser waveform and the apparent foliage profile. For this two-layered forest stand, the two species are independent of each other. The simulation

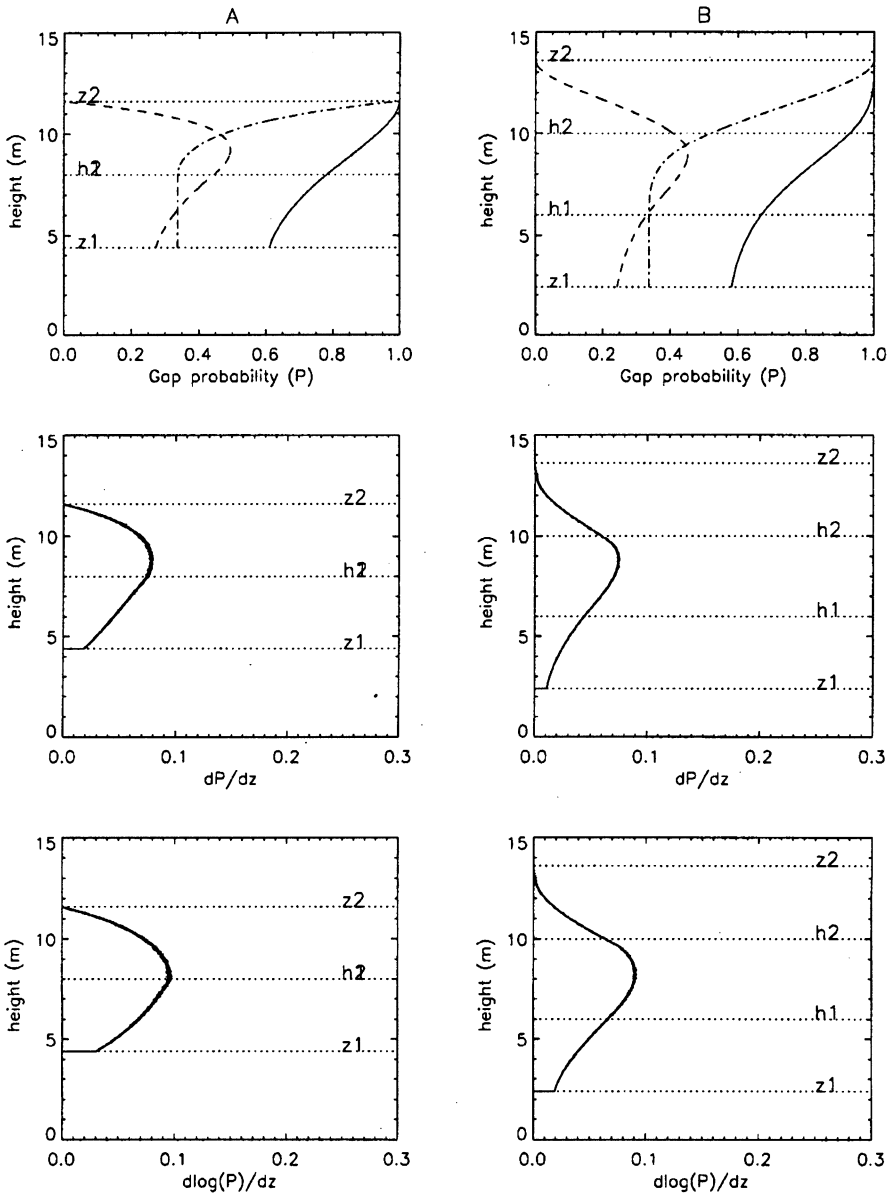

Fig. 4. Modeled vertical distribution of the gap probabilities $P(z)$ (solid line) [including between-crown gap probability, $P(n = 0, z)$ (dash-dot line), and within-crown gap probability, $P(n > 0, z)$ (dash line), $P(z) = P(n = 0, z) + P(n > 0, z)$], $dP(z)/dz$, and apparent foliage distribution, $(d\log(P(z))/dz)$, using the GORT model. The parameters used for case A and B are listed in Table I.

of the gap probability is straightforward. Simple multiplication of the two gap probabilities for the two species will do. In reality, due to ecological competition, the vertical distribution of different species may not be independent of each other.

IV. Model Validation

To access the performance of modeling the laser waveforms using the gap probability models presented above, we compared the model predictions with the SLICER data collected during the field campaign of BOREAS.

A. SLICER Data from BOREAS Site

BOREAS is a large-scale interdisciplinary experiment in central Canada focusing on improving our understanding of the interactions between the boreal forest biome and the atmosphere, and to clarify their role in global climate change [33]. During the BOREAS summer field campaign of 1996, SLICER was deployed on the NASA Wallops Flight Facility C-130 to measure the vertical structure of boreal forests and the topography of the underlying ground surface.

During the field campaign, intensive field measurements of tree geometry parameters [2], [22], the spectral properties of canopy elements [17], and the spectral properties of ground [18] were conducted. These ground measurements at four super study sites of BOREAS (Table III) were used to drive gap probability models.

A few concerns about the inputs need to be addressed. First, these measurements were conducted during the summer field campaign of 1994, but the SLICER data were collected during the summer field campaign of 1996. In this study, we ignore the small dynamic tree growth during the two-year period. Second,

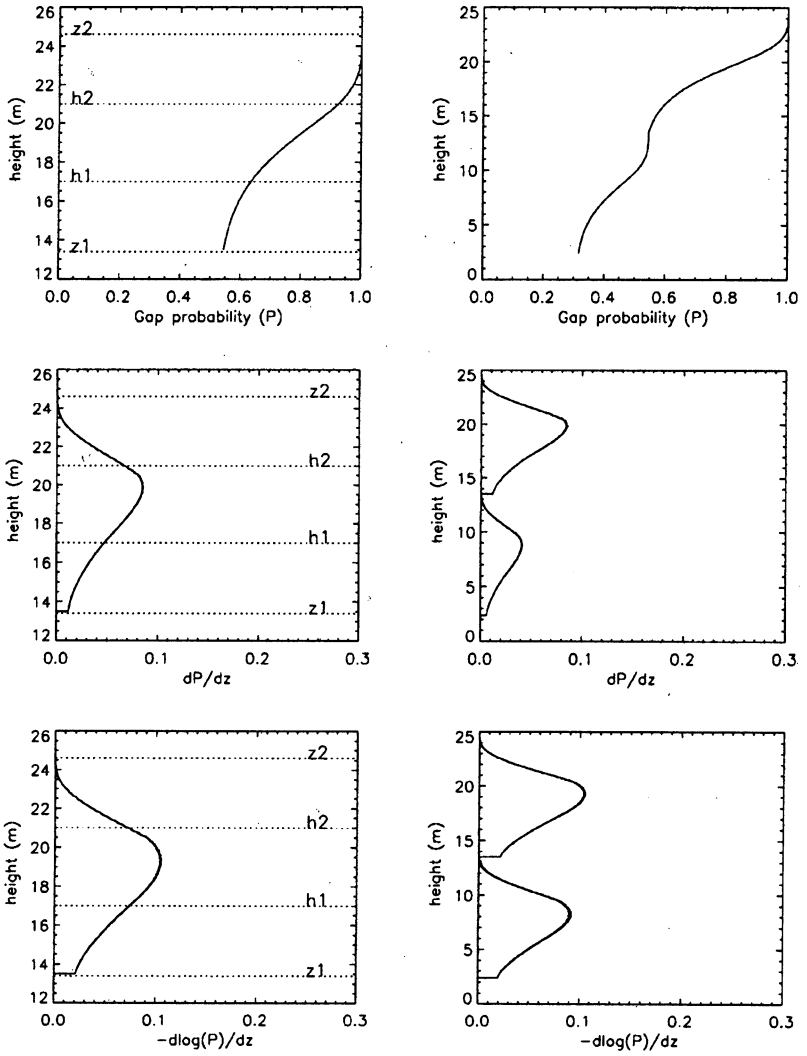

Fig. 5. Modeled vertical distribution of the gap probability $P(z)$, waveform $dP(z)/dz$, and foliage distribution $(d\log(P(z))/dz)$ using the GORT model (solid lines) for a broadleaf forest and two-layered forest (top layer: broadleaf tree stand, bottom layer: conifer tree stand).

TABLE II
INPUT TREE GEOMETRY PARAMETERS FOR THE GORT MODEL IN A BROADLEAF FOREST STAND

site	$R(m)$	$b(m)$	$\lambda(\frac{1}{m^2})$	$h_1(m)$	$h_2(m)$	$F_a(1/m)$
broadleaf	3.0	3.5	0.04	17	21	0.5

TABLE III
INPUT TREE GEOMETRY PARAMETERS FOR THE GORT MODEL IN THE FOUR CONIFER FOREST STANDS

site	$R(m)$	$b(m)$	$\lambda(\frac{1}{m^2})$	$\lambda_v(\frac{1}{m^3})$	$h_1(m)$	$h_2(m)$	$F_a(1/m)$	ω	ω_g
SOBS	0.76	2.65	0.405	0.074	3.03	8.5	0.87	0.8	0.303
SOJP	1.2	3.5	0.20	0.040	7.7	12.7	0.41	0.8	0.33
NOBS	1.0	3.5	0.24	0.037	5.5	12.0	0.44	0.8	0.317
NOJP	1.0	3.0	0.20	0.061	6.8	10.1	0.44	0.8	0.295

the spectral properties of canopy elements and the background, as shown in Table III, are at 0.9 μm. We use them at 1.06 μm which is the SLICER laser beam wavelength because of small

TABLE IV
TREE PARAMETER MEASUREMENTS BY [2]

site	age (yr)	tree ht. (m)	density$(\frac{1}{m})$
SOJP	60-75	12-15	0.16-0.24
SOBS	0-155	0-11	0.37-0.44
NOJP	50-65	9-13.5	0.13-0.26
NOBS	79-90	9-12	0.115-0.87

observed differences in the spectral properties between these two wavelengths [30], especially for conifer forests [5]. Third, the upper bound of tree crown centers h_2 is closely related to the tree height. As indicated in Chen's measurements (Table IV), the trees in the NOJP site are taller than those at the NOBS site. But our SLICER waveforms show the opposite (see Fig. 7). The value of h_2 for the NOBS site in Table III was therefore estimated from the SLICER waveform rather than Chen's measurements. We believe the SLICER height measurements are more accurate since Chen's measurement may have been conducted on a slightly different site. In the future, height derived directly

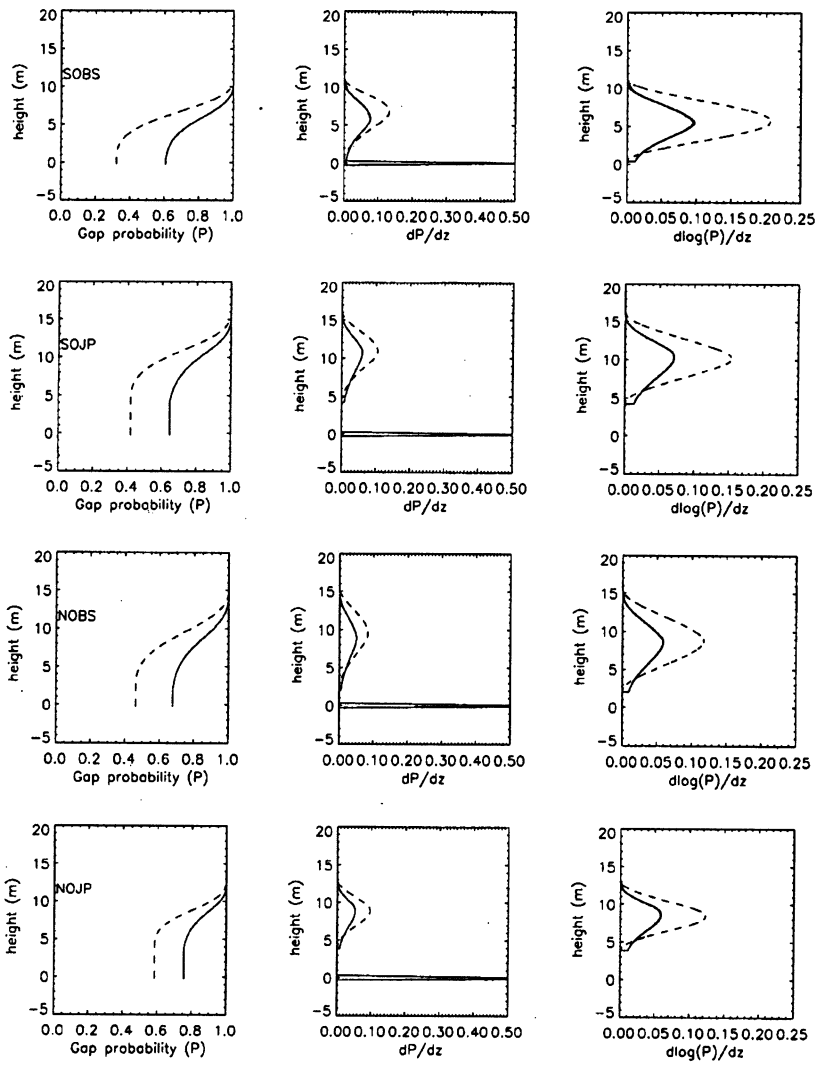

Fig. 6. Modeled vertical distribution of the gap probability $P(z)$, waveform $dP(z)/dz$, and apparent foliage profile $(d\log(P(z))/dz)$ for clumped forests (solid lines) and the horizontally homogeneous forests (dashed line). Four conifer forest stands of central Canada are used to represent the clumped forests. To make up a horizontally homogeneous canopy layer for the four conifer forests, the foliage elements within each thin layer are assumed to be horizontally distributed within each thin layer. The actual foliage profile for clumped forests and nonclumped forests are the same. SOBS: old black spruce forest stand in the southern super study site of BOREAS. SOJP: old jack pine forest stand in the southern super study site of BOREAS. NOBS: old black spruce forest stand in the northern super study site of BOREAS. NOJP: old old jack pine forest stand in the northern super study site of BOREAS. SOBS, SOJP, NOBS, and NOJP are with the same meanings in the following plots. It can be seen that the assumption of horizontally homogeneous plant canopies leads to underestimation of foliage area density.

from the laser data can be embedded in the inversion algorithm to reduce the uncertainty in the inversion outputs.

B. Model Predictions

Using the inputs provided in Table III, the GORT model was run to model gap probability for the four conifer forest stands. Fig. 6 shows the modeled vertical distribution of gap probability $P(z)$, $dP(z)/dz$, and apparent foliage profile $d\log(P(z))/dz$ in the SOBS, SOJP, NOBS, and NOJP sites. For comparison, horizontally homogeneous (no-clumped) forest stands are made up as if they had the same foliage profile as the four BOREAS super sites, but the foliage were randomly distributed horizontally. The actual vertical foliage profile is calculated using (34) and (35).

The first column in Fig. 6 shows the modeled gap probabilities in the four super sites. The gap probabilities in both the clumped and no-clumped forest stands show a sigmoid shape. But the ones for clumped forests are much larger than the nonclumped case. The largest difference is shown in the SOBS site, where the tree crowns and the foliage areas within crowns are the densest. The least difference is shown in the NOBS site, where the trees are the most sparsely distributed. Although there is not much difference in the tree shape, size, density for the NOBS and NOJP sites, the trees are much more widely distributed in the vertical direction at the NOBS site than at the NOJP site.

The middle column in Fig. 6 shows the modeled $dP(z)/dz$. A peak value is shown for all waveforms. The peak value seems located at a higher level for the nonclumped case than for the clumped forests. But the difference is not great. The peak values of the waveforms for the nonclumped cases are always larger than those for the clumped cases. The difference is greatest at the SOBS site and least at the NOBS site. This indicates that

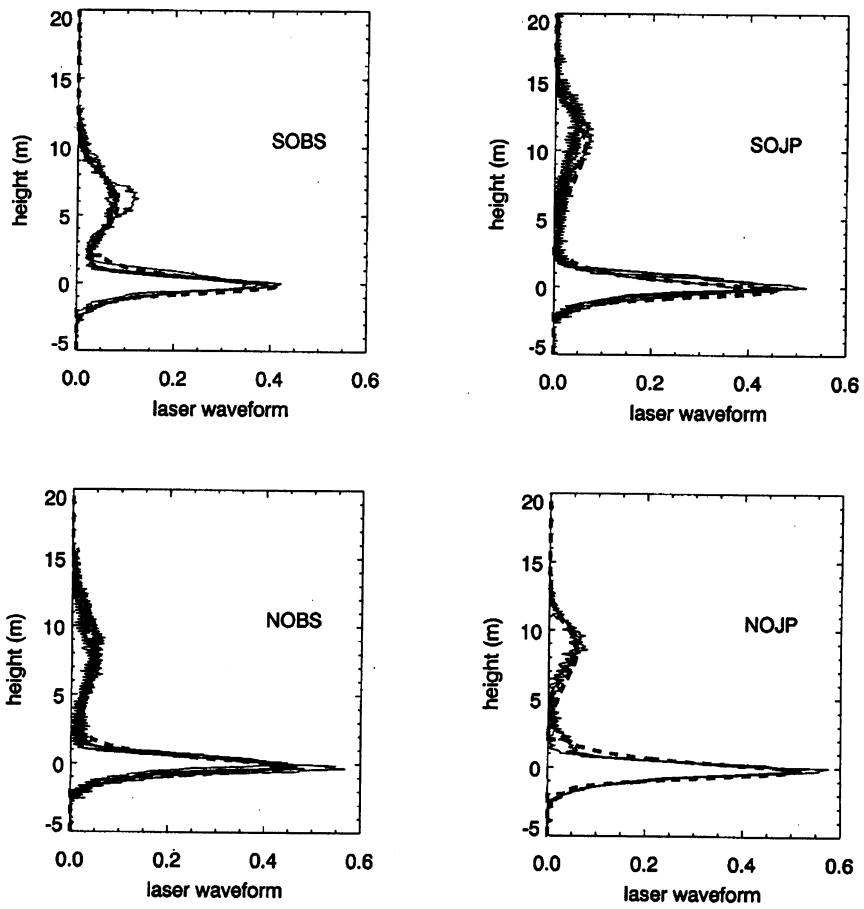

Fig. 7. Comparison of the modeled waveforms from the GORT model (thick-dashed lines) with the SLICER measurements (solid lines) in four conifer forest stands of central Canada.

the nonclumped forest stands lead to higher values of foliage profiles.

The rightmost column in Fig. 6 shows the retrieved apparent foliage profile using a simple logarithmic transformation of the gap probability. If we assume the leaf area projection factor is 1, the deviation of the apparent foliage profile for clumped forests from the one for nonclumped cases is the error of foliage profile retrieval arising from using the logarithmic transformation and ignoring the clumping effect for natural vegetation. The error is largest at the SOBS site, where the trees are most densely distributed. This shows that clumping still exists in some dense forests, which cannot be directly treated as horizontally homogeneous plant canopies for the retrieval of vertical foliage profile.

C. Model Comparison with SLICER Data

1) Waveform and Gap Probability Comparison: Fig. 7 shows the comparison between the modeled waveforms and the measurements from SLICER data at the four super study sites of BOREAS. The values of the waveforms from SLICER data are digitized counts density (digitized counts per unit height) normalized by the total digitized counts. The values of the waveforms predicted from the model are also normalized by the total laser energy return. Because of SLICER data are a convolution of an ideal impulse (zero width) laser pulse with a Rayleigh distribution of finite width, the modeled waveforms were also convoluted with a Rayleigh distribution of finite width. Good agreements between the modeled and measured waveforms are observed in Fig. 7.

The modeled gap probabilities and the retrieved gap probabilities from SLICER data are shown in Fig. 8. The modeled gap probabilities are close to the retrieved gap probabilities. In this study, we assume randomly oriented leaves, and the ratios of ρ_v/ρ_g are close to one in each case [see (17) and Table III for the spectral properties of leaves and background].

Figs. 7 and 8 also show that even within one forest stand site, the waveforms and the gap probabilities are not uniform. One waveform or gap probability deviates from others at the SOBS site. This might be due to different tree densities or different values of ρ_v/ρ_g at one forest stand or due to natural spatial variation in the sensing. The gap probabilities in the SOJP and the NOBS sites also do not have a uniform sigmoid shape. This might be the effect of different tree heights in the same forest stand or (again) simply spatial variation from sample to sample within a stand. Accounting for this variation will be important in future work.

Figs. 7 and 8 also show four different patterns in the modeled and SLICER-measured waveforms at the four super sites of BOREAS. Different tree heights in the four sites are the most

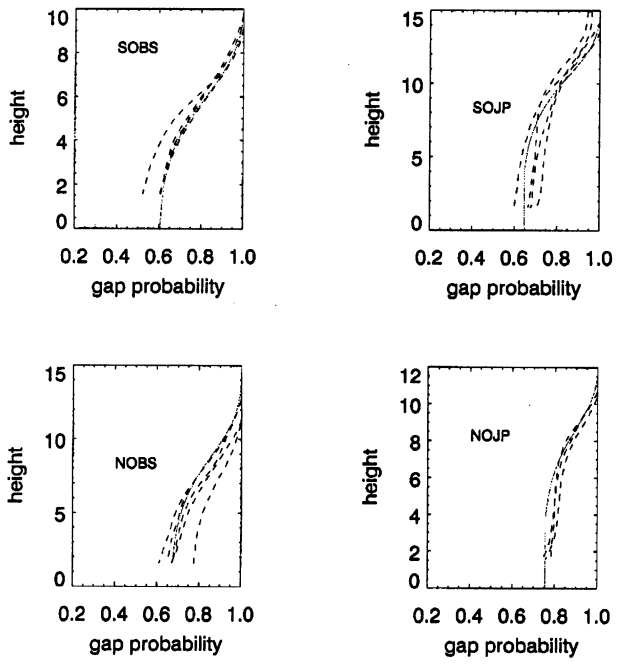

Fig. 8. Comparison of the modeled gap probabilities from the GORT model (solid lines) with the SLICER measurements (dashed lines) in four conifer forest stands of central Canada.

apparent. Different foliage profiles are also shown. Our experience of processing the SLICER data tells us that the waveforms are very sensitive to the tree geometry parameters. Within one SLICER flight for the same super site, the waveforms change dramatically. Laser waveforms are thus able to retrieve the spatial variability of vertical structure above the land surface. The agreement of the model prediction of the waveforms with the SLICER data in the four super sites indicates that the GORT model also catches the horizontal spatial variability of the canopy structure on the laser waveforms. Possibly, with some effort, the GORT model can be inverted to retrieve the spatial variability of the tree geometry parameters such as tree density or vertical foliage profile within a stand from lidar data.

2) Pulse Width and Footprint Size Effects on the Data: Canopy lidars generally have a finite pulse width. Its shape is part of the instrument design being a Rayleigh in the case of SLICER and a Gaussian in the case of LVIS and VCL. This effects the distribution of power across the footprint, and this must be taken into account.

Our experience with the Rayleigh or Gaussian smoothing on the laser pulse shows that the smoothing operation of the pulse does not damage the foliage profile interpretations, but rather usually improves retrievals through its smoothing action. However the main problem is the mixing of near ground foliage returns and the ground return. SLICER has a broad pulse so it is hard to distinguish real foliage effects near the ground from the ground pulse. It is therefore important either to fully "deconvolve" the effects of the pulse shape and width from the data or unmix the ground effect from the vegetation data. Both approaches are useful but will not be discussed further here.

The distribution of laser power over the footprint is not uniform but normally follows the TEM00 mode which follows a Gaussian distribution from the center of the footprint to the edge. The quoted "footprint" of SLICER, for example, [9] is the width to the point where the power falls to e^{-2} of its center level.

A narrow width of this Gaussian distribution of the laser pulse in space leads to a small effective footprint size with a consequent increase in spatial variance of the data. A small footprint, centimeters to several meters in diameter, may have just one signal returning from the first scattering event, with considerable attenuation for the remaining beam. For small spot sizes, the signal also often penetrates gaps in the canopy to give a clean, unattenuated and distinct surface background signal even with a significant overstory of trees. This is an advantage when the objective is terrain mapping. However, the disadvantage of the small footprint size for canopy lidar is that the gap probability can not be inferred except from a large number of samples. The spatial variance of returns may be so high that very large volumes of data will be needed to infer stable canopy parameters.

A large footprint size allows relatively stable estimates of the foliage profile and the gap probability function to be derived for each lidar pulse with an optimum spot size dependent on the canopy clump size and mapping scale and objectives. The spot size therefore might be varied as a function of land cover. If the spot size is too large, however, the return signals becomes a heterogeneous mixture. The 10–15 m footprint for SLICER and 25 m for LVIS/VCL are ideal for canopy applications since they match the tree stand scale. But the trade-off for large footprint size is that the signal from ground becomes mixed with the signal from canopy. This signal from ground can change its shape depending on micro-relief, slope and near surface corner reflections. However, provided this variation is not dominant, the GORT model presented here is well suited for interpreting lidar remote sensing data with a large footprint size.

Fortunately, the spatial variation introduced by the interaction of the cover with the lidar footprint can also be modeled with the GORT model (see [25]) allowing the effects of footprint size to be quantified and creating the potential to use the variation to infer canopy parameters.

3) Sensitivity of Gap Probability and Apparent Foliage Profile to ρ_v/ρ_g: For further analysis of the sensitivity of the retrieved gap probability, apparent foliage profile, and relative apparent foliage profile to the ratio of ρ_v/ρ_g, Fig. 9 shows one SLICER waveform from each supersite, the retrieved gap probability and apparent foliage profile with three values (0.75, 1, and 1.5) of ρ_v/ρ_g. A smaller value of ρ_v/ρ_g leads to a smaller gap probability, and to larger values of the apparent foliage profile. A large difference can be seen in the retrieved gap probabilities and the apparent foliage profiles when we use different values of ρ_v/ρ_g. Note that the amplifier $R_g/R_v(0)$ also affects the sensitivity of the retrieved gap probability and apparent foliage profile to ρ_v/ρ_g. Larger values of $R_g/R_v(0)$ amplify the sensitivity to ρ_v/ρ_g. Fig. 9 also shows that the relative foliage profile is not sensitive to the value of ρ_v/ρ_g.

Using our previous results it may be shown that the total projected cover estimate at the ground is

$$Cover(0) = \frac{1}{1 + \dfrac{\rho_v}{\rho_g}\dfrac{R_g}{R_v(0)}}. \tag{36}$$

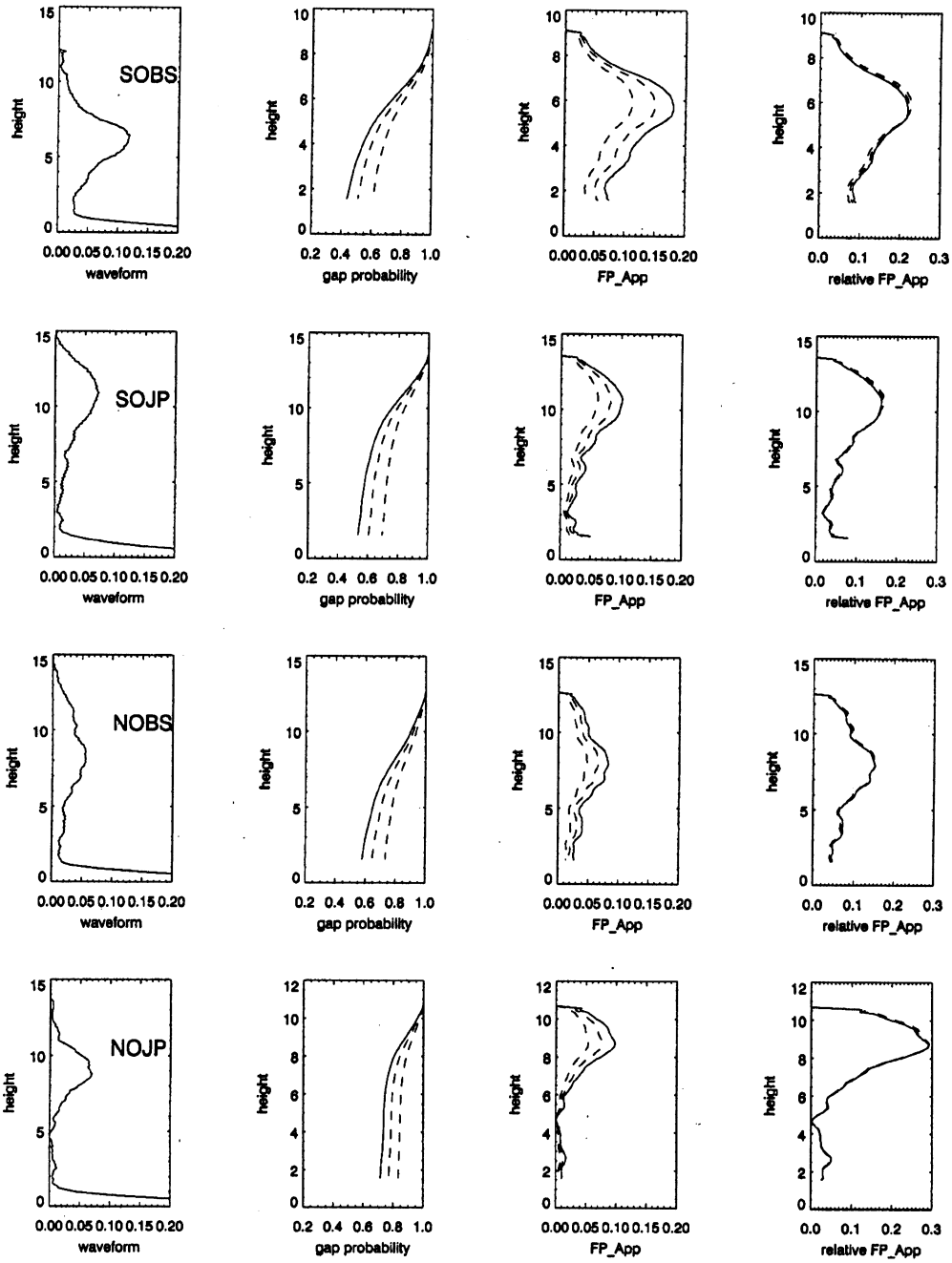

Fig. 9. Effect of the ratio of volume backscattering coefficient of vegetation and background on the retrieval of gap probability and apparent foliage profile in the four BOREAS super-sites. The SLICER waveforms are shown in column one, the retrieved gap probabilities in column two (dashed, dashed, solid lines for the ratios 1.5,1, and 0.75), and the retrieved apparent foliage profiles (APF) and relative APFs in column three and four (dashed, dashed, solid lines for the ratios 1.5, 1, and 0.75).

This shows that the main effect of a poor estimate in the ratio is to change the overall cover estimate.

V. Conclusions

Lidar measurements of vegetation canopy have a great potential for characterizing vertical canopy structure. This study has explored the relationship between the laser waveforms returned from plant canopies and vertical canopy structure parameters and how this relationship is affected by the spatial arrangements of canopy elements using a modeling approach. The effect of clumping of canopy elements, which occurs for most natural vegetation, on lidar waveforms and the foliage profile retrieval was studied using a geometric optical and radiative transfer model. Larger gap probability is observed for discontinuous plant canopies because of the clumping of leaves into crowns compared to horizontally homogeneous plant canopies. This clumping also generates smaller laser waveforms from above-ground foliage and woody elements and a larger laser return from the ground for discontinuous

plant canopies than horizontally homogeneous plant canopies with the same amount of foliage. Not accounting for the effect of clumping, the vertical foliage area density and the biomass for discontinuous plant canopies will therefore be underestimated using direct estimates such as a simple logarithmic transformation. In a sense, this represents a "hidden biomass" that potentially can be retrieved using a model such as GORT.

The GORT model was validated against independently measured field data using SLICER lidar data collected in conifer forest stands in Central Canada with good accuracy. The model validation shows that the GORT model is able to characterize the lidar waveform using a few tree geometry parameters, the spectral properties of canopy leaves, and the ground albedo.

Due to the clumping of leaves into crowns for natural vegetation, only the gap probability and apparent vertically projected foliage profile can be directly retrieved from the canopy lidar return. To achieve accuracy in such retrievals, a sensitive parameter: the ratio of the backscattering coefficient of the vegetation and the ground, which is a function of the leaf orientation factor, the spectral properties of the leaf and the ground, must be obtained independently. A sparse canopy and bright background reflectance will cause the retrieval to be most sensitive to the ratio.

The apparent foliage profile is generally different from the actual foliage profile. The difference is dependent on the leaf orientation factor and the clumping of vegetation. For horizontally homogeneous plant canopies, the actual foliage profile can be calculated by the ratio of the apparent foliage profile and the leaf orientation factor at nadir. For natural vegetation, besides the effect of the leaf orientation factor, the clumping of foliage into crowns leads to larger gap probability, and the values of the apparent foliage profile are smaller than the actual foliage profile; in other words, there is "hidden biomass."

For the possible retrieval of the actual foliage profiles and so biomass, suggestions are described as follows.

- Invert the GORT model to retrieve the tree density and foliage area volume density within crowns using lidar data first and calculate the actual foliage profile from the retrieved tree structure parameters. Some directly retrieved tree geometry parameters (such as tree height) from the laser returns can be used in the inversion to reduce the uncertainty of the inversion results.
- Make use of the spatial variance of the laser return. Developing a model for the vertical profile of spatial variance of gap probability can help us understand the spatial information of the laser returns. The spatial variation information provides us additional information on the canopy structure.
- Combine multiangular lidar measurements with nadir measurements. This may also provide us a way to retrieve directly the actual foliage profile, and especially the angular foliage distribution. A clumping index as a function of incident zenith angle is under development, which may link the apparent foliage profiles at different laser incident directions and the actual foliage profile.

These paths will be further explored in future work.

ACKNOWLEDGMENT

The authors would like to thank C. E. Woodcock, Boston University, Boston, MA, who pointed out the potential of applying the GORT Model to lidar data and for encouraging the pursuit of this direction. They would also like to thank D. Harding and M. Hofton for providing the SLICER data, and D. Harding and B. Blair for the useful discussion on how to process the SLICER data. They would also like to thank two reviewers for helpful comments.

REFERENCES

[1] G. S. Campbell and J. M. Norman, "The description and measurement of plant canopy structure," in *Plant Canopies: Their Growth, Form and Function*, R. Russell, B. Marshall, and P. G. Jarvis, Eds. Cambridge, MA: Cambridge Univ. Press, 1989.

[2] J. M. Chen, "Optically-based methods for measuring seasonable variation of leaf area index in boreal conifer stands," *Agric. Forest Meteorol.*, vol. 80, pp. 135–163, 1996.

[3] R. Dubayah, J. B. Blair, and J. L. Bufton *et al.*, "The vegetation canopy lidar mission," in *Land Satellite Information in the Next Decade II: Sources and Applications in ASPRS*, Washington, DC, 1997, pp. 11–112.

[4] R. Dubayah, R. Knox, M. Hofton, J. B. Blair, and J. Drake, "Land surface characterization using lidar remote sensing," in *Spatial Information for Land Use Management*, M. J. Hill and R. J. Aspinall, Eds. Sydney, Australia: Gordon and Breach, pp. 25–38.

[5] L. Dungan, L. Johnson, C. Billow, P. Matson, J. Mazzurco, J. Moen, and V. Vanderbilt, "High spectral resolution reflectance of Douglas Fir grown under different fertilization treatments: Experimental design and treatment effects," *Remote Sens. Environ.*, vol. 55, pp. 217–228, 1996.

[6] Space Appl. Inst., JRC, Eur. Comission, 1998.

[7] B. Hapke, "Bidirectional reflectance spectroscopy," *J. Geophys. Res.*, vol. 86, no. B4, pp. 3039–3054, 1981.

[8] D. J. Harding, M. A. Lefsky, G. G. Parker, and J. B. Blair, "Laser altimeter canopy height profiles: Methods and validation for closed-canopy, broadleaf forests," *Remote Sens. Environ.*, to be published.

[9] D. J. Harding, J. B. Blair, D. L. Rabine, and K. L. Still, "SLICER airborne laser altimeter characterization of canopy structure and sub-canopy topography for the BOREAS northern and southern study regions: Instrument and data product description," in *Series on the Boreal Ecosystem–Atmosphere Study (BOREAS): Remote Sensing Sciences Group*, F. Hall and J. Nickeson, Eds. Washington, DC: NASA/TM-2000-209 891.

[10] D. L. B. Jupp, "Spatial statistics in vegetation models,", 2000, submitted for publication.

[11] V. A. Kanevski, J. Ross, S. M. Kochubey, and T. Shadchina, "Laser remote sensing of vegetation," in *Advances in Bioclimatology*, Y. Cohen, J. M. Elwood, M. G. Holms, V. A. Kanevski, J. Ross, T. Shadchina, E. Simenson, and F. I. Woodward, Eds. Berlin, Germany: Springer-Verlag, 1994, vol. 3, pp. 90–124.

[12] M. A. Lefsky, D. Harding, W. B. Cohen, G. Parker, and H. H. Shugart, "Surface lidar remote sensing of basal area and biomass in deciduous forests of eastern Maryland, USA," *Remote Sens. Environ.*, vol. 67, pp. 83–98, 1999.

[13] M. A. Lefsky, W. B. Cohen, S. A. Acker, G. G. Parker, T. A. Spies, and D. Harding, "Lidar remote sensing of the canopy structure and biophysical properties of Douglas-fir western hemlock forests," *Remote Sens. Environ.*, vol. 70, pp. 339–361, 1999.

[14] R. H. MacArthur and H. S. Horn, "Foliage profile by vertical measurements," *Ecology*, vol. 50, pp. 802–804, 1969.

[15] L. A. McDade, K. S. Bawa, H. A. Hespenheide, and G. S. Hartshorn, Eds., *La Selva—Ecology and Natural History of a Neotropical Rain Forest*. Chicago, IL: Univ. Chicago Press, 1994.

[16] J. E. Means, S. A. Acker, D. J. Harding, J. B. Blair, M. A. Lefsky, W. B. Cohen, M. E. Harmon, and W. A. McKee, "Use of large-footprint scanning airborne lidar to estimate forest stand characteristics in the Western Cascades of Oregon," *Remote Sens. Environ.*, vol. 67, pp. 298–308, 1999.

[17] E. M. Middleton and E. A. Walter-Shea, "Optical properties of canopy elements in the boreal forest," in *Int. Geoscience and Remote Sensing Symp.*, 1995, pp. 789–793.

[18] J. R. Miller, H. P. White, J. M. Chen, D. R. Peddle, G. McDermid, R. A. Fournier, P. Shepherd, I. Rubinstein, J. Freemantle, R. Soffer, and E. LeDrew, "Seasonal change in understory reflectance of boreal forests and influence on canopy vegetation indices," *J. Geophys. Res.*, vol. 102, no. D24, pp. 29 729–29 736, 1997.
[19] T. Y. Nakajima, O. Uchino, T. Nagai, and T. Moriyama, "Possibility of cloud and aerosol observations by spaceborne mie lidar," in *Proc. IRS'96, Current Problems in Atmospheric Radiation*, W. Smith and K. Stamnes, Eds., Fairbanks, AK, Aug. 19–24 1996.
[20] E. Nasset, "Estimating timber volume of forest stands using airborne laser scanner data," *Remote Sens. Environ.*, vol. 61, pp. 246–253, 1997.
[21] R. Nelson, "Modeling forest canopy heights: The effects of canopy shape," *Remote Sens. Environ.*, vol. 60, pp. 327–334, 1997.
[22] W. Ni, X. Li, C. E. Woodcock, J. L. Roujean, and R. Davis, "Transmission of solar radiation in boreal conifer forests: Measurements and models," *J. Geophys. Res.*, vol. 102, no. D24, pp. 29 555–29 566, 1997.
[23] W. Ni, X. Li, C. E. Woodcock, M. R. Caetano, and A. H. Strahler, "An analytical hybrid GORT bidirectional reflectance model for discontinuous plant canopies," *IEEE Trans. Geosci. Remote Sensing*, vol. 37, pp. 987–999, Mar. 1999.
[24] W. Ni, C. E. Woodcock, and D. L. B. Jupp, "Variance in bidirectional reflectance over discontinuous plant canopies," *Remote Sens. Environ.*, vol. 69, pp. 1–15, 1999.
[25] W. Ni and D. L. B. Jupp, "Spatial variance in directional remote sensing imagery—Recent developments and future perspectives," *Remote Sensing Rev.*, vol. 18, no. 2–4, pp. 441–479, 2000.
[26] W. Ni and C. E. Woodcock, "The effect of canopy structure and the presence of snow on the albedo of boreal conifer forests," *J. Geophys. Res.*, vol. 105, no. D9, pp. 11 879–11 888, 2000.
[27] W. Ni and X. Li, "A coupled vegetation-soil bidirectional reflectance model for a semi-arid landscape," *Remote Sens. Environ.*, vol. 74, pp. 113–124, 2000.
[28] M. Nilson, "Estimation of tree heights and stand volume using an airborne lidar system," *Remote Sens. Environ.*, vol. 56, pp. 1–7, 1995.
[29] G. Roberts, "Simulating the vegetation canopy lidar: An investigation of the waveform information content," submitted as part of requirement for the M.Sc. in remote sensing, Univ. College, London, U.K., 1998.
[30] J. K. Ross, *The Radiative Regime and Architecture of Plant Stands*. The Hague, The Netherlands: Dr. W. Junk, 1981, p. 391.
[31] J. L. Roujean, "A tractable physical model of shortwave radiation interception by by vegetation canopies," *J. Geophys. Res.*, vol. 101, pp. 9523–9532, 1996.
[32] J. Serra, *Image Analysis and Mathematical Morphology*. New York: Academic, 1982.
[33] P. Sellers, F. M. Hall, D. B. Kelly, D. Baldocchi, and G. den Hartog *et al.*, "The boreal ecosystem-atmosphere study (BOREAS): An overview and early results from the 1994 field year," *Bull. Amer. Meteorol. Soc.*, vol. 76, pp. 1549–1577, 1995.
[34] G. Sun and K. J. Ranson, "Modeling lidar returns from forest canopies," *IEEE Trans. Geosci. Remote Sensing*, to be published.
[35] X. Li, A. H. Strahler, and C. E. Woodcock, "A hybrid geometric optical-radiative transfer approach for modeling albedo and directional reflectance of discontinuous canopies," *IEEE Trans. Geosci. Remote Sensing*, vol. 33, pp. 466–480, Mar. 1995.

Wenge Ni-Meister received the Ph.D. degree in remote sensing from Boston University, Boston, MA, in 1997.

Currently, she is with the Goddard Earth Sciences and Technology Center, NASA Goddard Space Flight Center, Greenbelt, MD. Her interestes are land–atmosphere interactions, parameterizations of land surface processes for GCM, data assimilation, and carbon modeling and retrieval from remote sensing.

David L. B. Jupp is currently the Head of CSIRO Office of Space Science and Applications (COSSA) and Science Leader of the CSIRO Earth Observation Centre, Canberra, Australia. From 1980 to 1995, he was the Leader of Hydrological Remote Sensing, CSIRO Division of Water Resources. His work has involved negotiation, management, and completion of a broad range of projects involving research, applications, technology transfer, and commercialization of remote sensing methods, software and integration for land and water resource mapping and monitoring, and team building to ensure the success of the projects and applications has been a major activity. His research interests are in image processing and remote sensing; the mathematics of modeling and (geo-) physical inversion; physical modeling of radiation in the atmosphere, oceans, estuaries, rivers and inland waters and the land surface; physics of radiation in water bodies for applications of optical water quality and benthic mapping; computer systems analysis and programming; and remote sensing applications management and execution. He has worked on coastal zone and inland waters remote sensing; reef mapping in the Great Barrier Reef of Australia; airborne remote sensing of water quality, algal blooms and benthic vegetation; water resources applications; user training with the microBRAIN image processing system; NOAA AVHRR thermal data analysis of the land surface temperature for water resources applications to soil moisture and water balance estimation in the Murray Darling Basin of Australia; and international collaboration with Thailand, China, Indonesia, Canada, and the USA. For nine years, he was involved in the commercialization of the microBRAIN image processing system including software support and development, documentation, training, and user support. Recent involvement in the commercial development of a software and methods system to apply airborne imaging data for mapping and monitoring in southeast Asia.

Dr. Jupp was awarded the CSIRO Medal for Research Achievement in 1986 for leading research, applications, and technology transfer relating to the mapping of the Great Barrier Reef using satellite data.

Ralph Dubayah received the A.B. degree in geography from the University of California, Berkeley, in 1981, and the M.A. and Ph.D. degrees in geography from the University of California, Santa Barbara, in 1985 and 1991, respectively.

He is currently an Associate Professor in the Department of Geography, University of Maryland, College Park. His research interests include climatology, land surface characterization, macroscale hydrology, spatial analysis, and remote sensing. He was the Principal Investigator of the Vegetation Canopy Lidar (VCL) Mission, a collaboration between NASA and the University of Maryland, to map the vertical structure of the Earth's forests using a space-based lidar system.

Dr. Dubayah served as Chair of the Remote Sensing Committee of the American Geophysical Union from 1997 to 2000.